The Impact of Temperature and Switching Rate on the Dynamic Characteristics of Silicon Carbide Schottky Barrier Diodes and MOSFETs

Saeed Jahdi, *Student Member, IEEE,* Olayiwola Alatise, Petros Alexakis, *Student Member, IEEE,* Li Ran, *Senior Member, IEEE,* and Philip Mawby, *Senior Member, IEEE*

***Abstract*—SiC Schottky Barrier Diodes (SBDs) are prone to electromagnetic oscillations in the output characteristics. The oscillation frequency, peak voltage overshoot and damping are shown to depend on the ambient temperature and the MOSFET switching rate (dI_{DS}/dt). In this paper, it is shown experimentally and theoretically that dI_{DS}/dt increases with temperature for a given gate resistance during MOSFET turn-ON and reduces with increasing temperature during turn-OFF. As a result of this, the oscillation frequency and peak voltage overshoot of the SiC-SBD increases with temperature during diode turn-OFF. This temperature dependency of the diode ringing reduces at higher dI_{DS}/dt and increases at lower dI_{DS}/dt. It is also shown that the rate of change of dI_{DS}/dt with temperature ($d^2I_{DS}/dtdT$) is strongly dependent on R_G and using fundamental device physics equations, this behavior is predictable. The dependence of the switching energy on dI_{DS}/dt and temperature in 1.2 kV SiC-SBDs is measured over a wide temperature range (–75 °C to 200 °C). The diode switching energy analysis shows that the losses at low dI_{DS}/dt are dominated by the transient duration and losses at high dI_{DS}/dt are dominated by electromagnetic oscillations. The model developed and results obtained are important for predicting EMI, reliability and losses in SiC MOSFET/SBDs.**

***Index Terms*—Power MOSFET, Schottky diodes, Silicon carbide, Temperature, Oscillation**

I. Introduction

SILICON CARBIDE unipolar devices have now become commercially available with voltage ratings of 1.2 kV and higher voltage ratings are expected in the near future [1]–[5]. These temperature rugged and power dense devices have repeatedly demonstrated improved energy conversion efficiency and reduced losses when implemented in power converters [6]–[13]. Since these devices are unipolar and are therefore not limited by minority carrier storage from conductivity modulation, they are fast switching and can thus be implemented in high frequency applications. High switching frequency can enable size reduction of passive components which is a significant advantage in applications where space or size is critical to cost. This may include aeronautical and marine applications. However, advances in packaging technologies are not catching up with devices. Parasitic inductances in power modules induce electromagnetic oscillations in output characteristics which can be detrimental through the additional losses and reduced reliability [14]–[18]. These parasitic inductances depend strongly on the architecture of the power module and its layout. However, as the switching frequency increases, even small parasitic inductances cannot be ignored because of the high dI_{DS}/dt. It is well understood that SiC Schottky diodes are particularly prone to ringing as parasitic capacitances and inductances interact to cause RLC resonance [19]. The dependence of this ringing on the ambient temperature and the rate of change of current with time (dI_{DS}/dt) of the switching MOSFET has not been fully characterized and understood. The deployment of these 1.2 kV SiC power devices in hard-switched high temperature modules will require more understanding in the dependence of switching energy on temperature and switching rate [20]. A solution to this ringing problem could be the use of soft-switching techniques where zero current and/or zero voltage switching can be implemented. However, this will increase the cost and complexity of converters at the power levels targeted by SiC.

In this paper, 1.2 kV SiC MOSFETs and SiC Schottky diodes have been tested in a clamped inductive switching test rig. The devices have been tested with a wide range of gate resistances (10 Ω to 1000 Ω) at ambient temperatures ranging from –75 °C to 200 °C. Using fundamental device equations, the dependence of dI_{DS}/dt on the temperature and gate resistance is derived and shown to accurately replicate the experimental measurements. This temperature dependence is used to explain the performance of the Schottky diode in terms of energy losses. In Section II of this paper, the experimental measurements are presented. In Section III, the MOSFET switching and diode models are presented and compared with the experimental measurements. In Section IV, the switching performance of the silicon carbide Schottky barrier diode is analyzed while Section V concludes the paper.

II. Clamped Inductive Switching Measurements and Experimental Test Rig Design

The clamped inductive switching test rig comprises of the devices under test (1.2 kV/30 A SiC MOSFETs and diodes),

Manuscript received July 27, 2013; revised November 7, 2013, February 26, 2014; accepted April 12, 2014.

This work was supported in part by Science City Research Alliance.

The authors are with the Department of Electrical and Electronics Engineering, School of Engineering, University of Warwick, Coventry, West Midlands, CV4 7AL, United Kingdom (e-mail: s.jahdi@warwick.ac.uk, o.alatise@warwick.ac.uk, p.alexakis@warwick.ac.uk, l.ran@warwick.ac.uk, p.a.mawby@warwick.ac.uk)

a 7.4 mH commutation inductor, gate drive system and a power supply. A schematic of the test set-up is shown in Figure 1. Shown in Figure 2 is a picture of the test rig. The SiC MOSFET has the datasheet reference of SCH2080KE while the SiC Schottky Diode is SDP30S120.

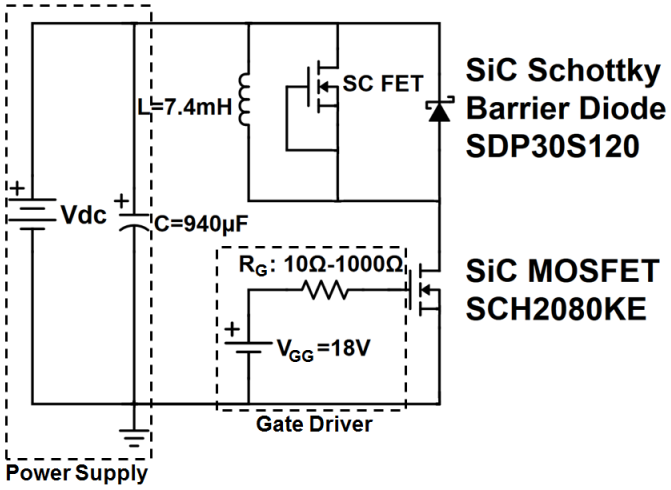

Fig. 1. Clamped Inductive Switching Test Rig Schematic

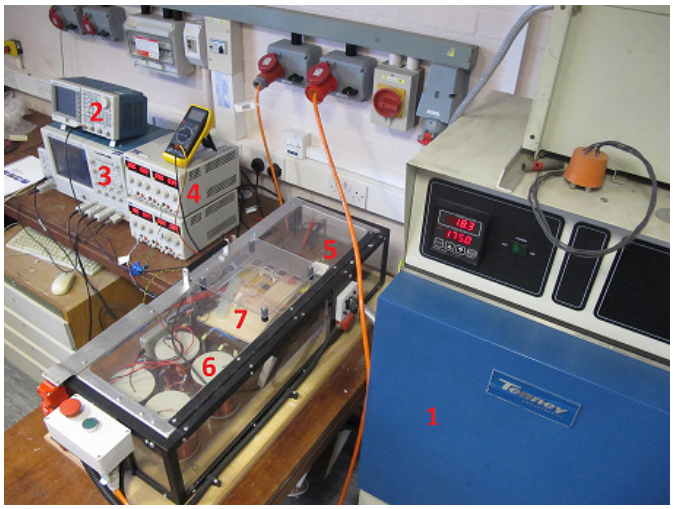

Fig. 2. Quasi-Switching Test Rig Components: 1- Thermal Chamber 2-Function Generator 3- Digital Oscilloscope 4- Gate Drive Power Supplies 5-Bank Capacitors 6-Inductors 7-Gate Drive System

The switching waveforms were captured on a Tektronix TDS5054 digital phosphor oscilloscope which has a bandwidth of 500 MHz and the static characteristics were measured on a Tekronix curve tracer. The current is measured using a Tekronix TCP303 current probe connected to the oscilloscope. This circuit emulates one phase-leg of a 3 phase voltage source converter in which free-wheeling diodes (FWD) conduct current in the opposite direction to the MOSFET i.e. the diodes rectify while the MOSFETs invert. The environmental chamber shown in Figure 2 is a Tenney Environment chamber being able to vary the temperature within a range of –75 °C to 200 °C. The measurements here have been performed at a temperature range between –75 °C to 200 °C. Therefore the measurements have been performed at the above mentioned temperature range. However, for higher temperatures and harsh environments such as in aeronautical applications, bare dies should be packaged exclusively. It should be noted that emergence of SiC devices have raised the high temperature expectations considerably as they are proven to act better in such conditions compared to their silicon counterparts [21]–[24]. The power supply provides the charge voltage and the inductor is pre-charged to enable continuous current through the MOSFET/FWD arrangement. This is achieved by using the double pulse technique where the MOSFET is initially switched ON to charge the inductor to a defined current level before the main switching test is performed. The gate of the MOSFET is driven by a gate drive circuit comprised of a voltage source, a pulse generator and an optocoupler chip jointly supplying 18 V through the gate resistor for a period of 20 μs. When the MOSFET is switched OFF, majority of the supply voltage falls across it hence the FWD is forward biased and conducting. The voltage drop across the FWD during this phase will be due to its on-state resistance. As the MOSFET is switched ON and starts conducting, the current is commutated away from the FWD and the voltage across the MOSFET starts to fall to its on-state voltage drop. This causes the FWD to become reverse biased and blocking.

III. Model Development

The dependence of the turn-ON dI_{DS}/dt on temperature can be accounted for using the fundamental device equations. The MOSFET and the diode share the same total inductor current, hence, the turn-ON of the MOSFET and turn-OFF of the diode occurs within the same switching transient. Equation (1a) below is the gate charging transient characteristic during turn-ON (Equation (1b) is for turn-OFF) where V_{GS} is the gate-source voltage, V_{GG} is the gate driver voltage, R_G is the gate resistance, t is time and C_{iss} is the input capacitance.

$$V_{GS} = V_{GG}\left(1 - exp\left(-\frac{t}{R_G C_{iss}}\right)\right) \tag{1a}$$

$$V_{GS} = V_{GG}\, exp\left(-\frac{t}{R_G C_{iss}}\right) \tag{1b}$$

The rate of change of V_{GS} with time (dV_{GS}/dt) is evaluated simply by taking the derivative of (1a) with time for turn-ON and (1b) for turn-OFF which results in:

$$\left.\frac{\mathrm{d}V_{GS}}{\mathrm{d}t}\right|_{ON} = \frac{V_{GG}}{R_G C_{iss}} exp\left(-\frac{t}{R_G C_{iss}}\right) \tag{2a}$$

$$\left.\frac{\mathrm{d}V_{GS}}{\mathrm{d}t}\right|_{OFF} = -\frac{V_{GG}}{R_G C_{iss}} exp\left(-\frac{t}{R_G C_{iss}}\right) \tag{2b}$$

Equation (3) is the well-known equation for the drain current of a fully inverted long channel MOSFET in saturation.

$$I_{DS} = \frac{B}{2}\left(V_{GS} - V_{TH}\right)^2 \tag{3}$$

where

$$B = \frac{W\mu C_{OX}}{L}$$

V_{TH} is the threshold voltage, W is the width of the device, μ is the effective mobility of the carriers, C_{OX} is the effective capacitance density of the gate insulator and L is the channel length of the device. Taking the derivative of (3) with respect to time and substituting dV_{GS}/dt yields dI_{DS}/dt as shown below in (4a) for turn-ON and (4b) for turn-OFF.

$$\left.\frac{\mathrm{d}I_{DS}}{\mathrm{d}t}\right|_{ON} = B\left(V_{GS} - V_{TH}\right)\frac{V_{GG}}{R_G C_{iss}}\, exp(\frac{-t}{R_G C_{iss}}) \quad (4a)$$

$$\left.\frac{\mathrm{d}I_{DS}}{\mathrm{d}t}\right|_{OFF} = B\left(V_{GS} - V_{TH}\right)\frac{-V_{GG}}{R_G C_{iss}}\, exp(\frac{-t}{R_G C_{iss}}) \quad (4b)$$

where the threshold voltage (V_{TH}) and its temperature dependency is given by [25] as:

$$V_{TH} = V_{FB} + \frac{2KT}{q}\, ln(\frac{N_A}{n_i}) + \frac{\sqrt{4\epsilon_{si}KTN_A ln(\frac{N_A}{n_i})}}{C_{OX}} \quad (5)$$

In (5) above, N_A is the p-body doping, n_i is the intrinsic carrier concentration, C_{OX} is the oxide capacitance density of the gate dielectric and V_{FB} is the flat-band voltage (due to fixed oxide charge and the metal-semiconductor work-function difference). Equations (4a) and (4b) predict that dI_{DS}/dt will increase with temperature during turn-ON and decrease with temperature during turn-OFF. This is due to the negative temperature coefficient of the MOSFET threshold voltage as a result of thermally induced bandgap narrowing. As a result, V_{TH} will reduce at higher temperatures hence, dI_{DS}/dt will increase during turn-ON and decrease during turn-OFF according to (4). The experimental measurements of dI_{DS}/dt shown in Figure 3 for turn-ON and Figure 4 for turn-OFF agree with the trends predicted by Equations (4a) and (4b). In these figures, the temperature of the thermal chamber that houses the devices is set to 25 °C. Figure 3 shows measurements and calculations of the turn-ON dI_{DS}/dt as a function of R_G for the SiC MOSFETs. The calculations are based on values taken from the SCH2080KE datasheet as C_{iss} = 2nF, the threshold voltage at 25 °C is 5 V and B ranges from 0.5 to 1. The values of t used in the calculations in (4a) and (4b) correspond to the switching time value at which dI_{DS}/dt is calculated and V_{GS} is calculated from the equation of the plateau voltage (V_{GP}). The plateau voltage is calculated using the standard equations from [25] and it is assumed that the current switches between the time taken for V_{GS} to rise from V_{TH} to V_{GP} during turn-ON and fall from V_{GP} to V_{TH} during turn-OFF. The measurements and calculations show good agreement over the wide range of R_G as can be seen in Figure 3. Figure 4 shows the measurements and calculations of dI_{DS}/dt as a function of R_G during turn-OFF. There is reasonably good agreement between the measured and calculated trends however, there is some measurement noise which introduces some error especially at faster switching speeds. The rate of change of dI_{DS}/dt with respect to R_G can be evaluated by taking the derivative of (4) with respect to R_G. This derivative is shown in (6) below for turn-ON. In the case of the turn-OFF, (6) is simply multiplied by –1.

$$\frac{\mathrm{d}^2 I_{DS}}{\mathrm{d}t\mathrm{d}R_G} = B\left(V_{TH} - V_{GS}\right)\frac{V_{GG}}{R_G^2 C_{iss}} exp\left(-\frac{t}{R_G C_{iss}}\right)\left(\frac{t}{R_G C_{iss}} - 1\right) \quad (6)$$

The dependence of $d^2I_{DS}/dtdR_G$ on R_G can be observed by plotting the latter as a function of the former which is shown for the measurements and calculations in Figure 5 for turn-ON and Figure 6 for turn-OFF. Figure 5 shows good agreement between the experimental measurements and the calculations for turn-ON based on (6). Again, in Figure 6, there is some disparity at low R_G.

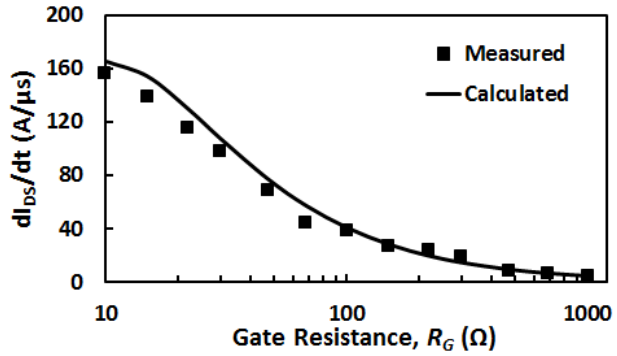

Fig. 3. Turn-ON dI_{DS}/dt as a function of R_G for measurements at 25 °C.

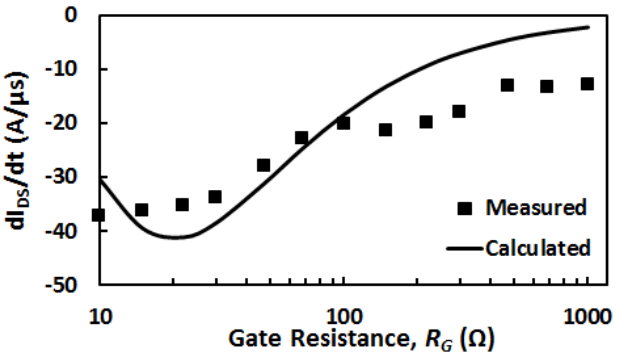

Fig. 4. Turn-OFF dI_{DS}/dt as a function of R_G for measurements at 25 °C.

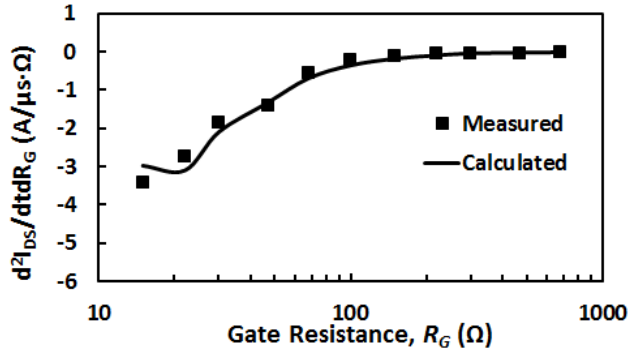

Fig. 5. Turn-ON $d^2I_{DS}/dtdT$ as a function of R_G for measurements at 25 °C.

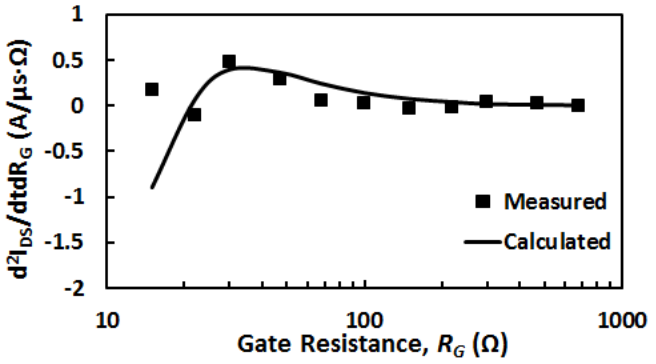

Fig. 6. Turn-OFF $d^2I_{DS}/dtdT$ as a function of R_G for measurement at 25 °C.

The temperature dependence of dI_{DS}/dt can be evaluated by taking the derivative of (4) with respect to temperature noting that V_{TH} is temperature dependent through the intrinsic carrier concentration as shown in (5) and B is temperature dependent through the effective mobility. For turn-ON, the derivative of (4a) with respect to temperature (T) is (7) below. For turn-OFF, (7) can simply be multiplied by –1.

$$\frac{\mathrm{d}^2 I_{DS}}{\mathrm{d}t\,\mathrm{d}T} = \frac{V_{GG}}{R_G\,C_{iss}}\,exp\left(-\frac{t}{R_G\,C_{iss}}\right) \left((V_{GS}-V_{TH})\,\frac{\mathrm{d}B}{\mathrm{d}T} - B\frac{\mathrm{d}V_{TH}}{\mathrm{d}T}\right) \tag{7}$$

In SiC MOSFETs, V_{TH} has a negative temperature coefficient as a result of thermally generated carriers due to bandgap narrowing (dV_{TH}/dT is negative) and B (which depends on the on-state resistance) is invariant with respect to temperature at low temperatures. This negative temperature coefficient of the threshold voltage can be seen in (5) and is due to the intrinsic carrier concentration (n_i) which increases with temperature due to increased thermal generation of carriers across the bandgap. Hence, according to (5), V_{TH} reduces as n_i increases. At higher temperatures dB/dT is negative as a result of the temperature dependence of the effective mobility i.e. phonon scattering induced mobility degradation reduces the effective mobility as the temperature is increased. Hence (7) can be re-written for low temperatures as:

$$\frac{\mathrm{d}^2 I_{DS}}{\mathrm{d}t\,\mathrm{d}T} = \frac{V_{GG}}{R_G\,C_{iss}}\,exp\left(-\frac{t}{R_G\,C_{iss}}\right)\left(B\left|\frac{\mathrm{d}V_{TH}}{\mathrm{d}T}\right|\right) \tag{8}$$

In the case of turn-OFF, (8) is multiplied by –1. It can be seen from (8) that dI_{DS}/dt increases with increasing temperature during turn-ON since the 2nd order derivative is positive and dI_{DS}/dt decreases with increasing temperature during turn-OFF since the 2nd order derivative is negative. Figure 7 shows the measured turn-ON dI_{DS}/dt as a function of R_G for different temperatures ranging from –75 °C to 200 °C whereas Figure 8 shows the measured turn-ON dI_{DS}/dt as a function of temperature for different gate resistances. It can be seen from Figure 7 and 8 that dI_{DS}/dt increases with temperature during turn-ON in agreement with (7) and (8); however, the rate of change of dI_{DS}/dt with temperature is not uniform for all the gate resistors. This trend can also be observed in other published reports on the performance of SiC MOSFETs at different temperatures where dI_{DS}/dt can be seen to increase with temperature during turn-ON [26], [27] or $|dV_{DS}/dt|$ (meaning the absolute value, i.e. the magnitude of dV_{DS}/dt) is shown in increase with temperature at turn-ON [28].

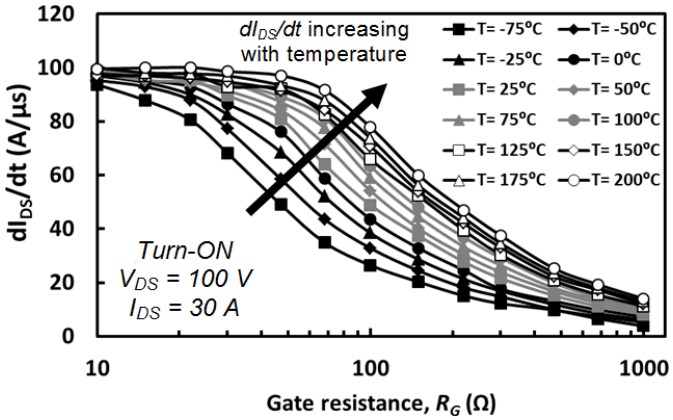

Fig. 7. Measured dI_{DS}/dt as a function of R_G at different temperatures during turn-ON.

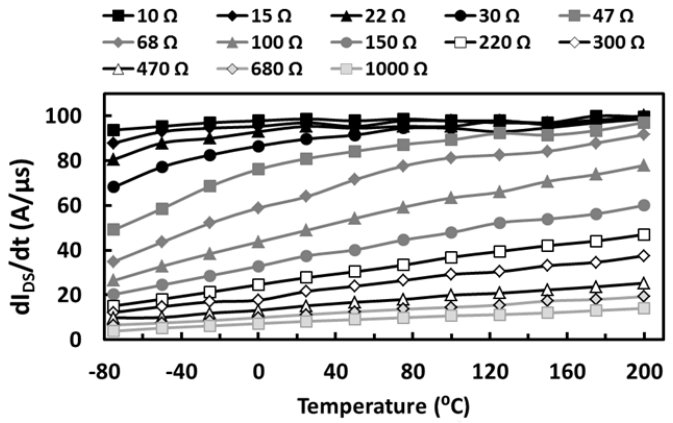

Fig. 8. Measured dI_{DS}/dt as a function of temperature for different gate resistances during turn-ON.

Figure 9 shows the turn-OFF $|dI_{DS}/dt|$ (meaning the absolute value, i.e. the magnitude of dI_{DS}/dt) as a function of R_G for different temperatures where it can be seen that dI_{DS}/dt decreases with increasing temperature as predicted by (7) and (8). Figure 9 shows the turn-OFF dI_{DS}/dt as a function of temperature for the different gate resistances. The dependence of $d^2I_{DS}/dtdT$ on R_G can further be considered by looking at how the former changes with respect to the latter. Figure 11 shows experimental measurements of the turn-ON $d^2I_{DS}/dtdT$ as a function of R_G for the different ambient temperatures. It can be seen from the measurements in Figure 11 that the variation of dI_{DS}/dt with temperature is small at larger and smaller values of R_G ($d^2I_{DS}/dtdT$ is small) and is much larger at intermediate values of R_G ($d^2I_{DS}/dtdT$ is larger) i.e. $d^2I_{DS}/dtdT$ as a function of R_G exhibits a bell shaped characteristic. Figure 12 shows the calculated $d^2I_{DS}/dtdT$ dT as a function of R_G at the different temperatures using (7) and (8) where the same bell shaped characteristic can be observed at

different temperatures. It can also be seen from Figure 11 that the maximum turn-ON $d^2I_{DS}/dtdT$ decreases as temperature increases. Equations (7) and (8) explain this behavior. It can be seen from (7) and (8) that as R_G is reduced, V_{GG}/R_GC_{iss} rises and $exp(-t/R_GC_{iss})$ reduces. Hence, a plot of $d^2I_{DS}/dtdT$ as a function of R_G will show a bell shaped characteristic as a result of the competing effects.

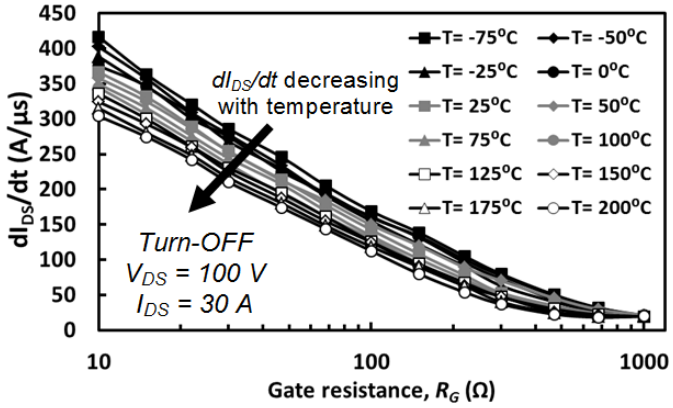

Fig. 9. Measured dI_{DS}/dt as a function of R_G at different temperatures during turn-OFF.

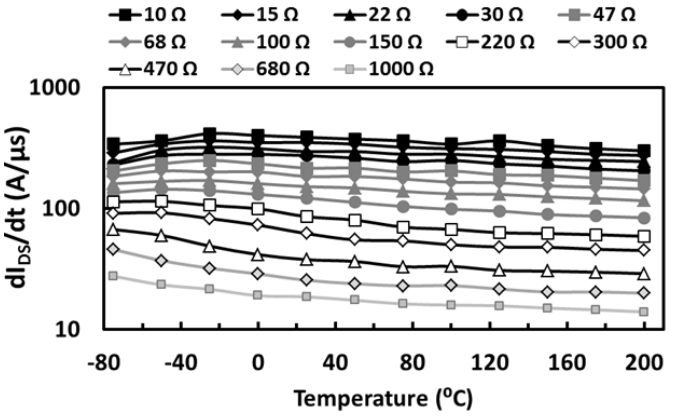

Fig. 10. Measured dI_{DS}/dt as a function of temperature for different gate resistances during turn-OFF.

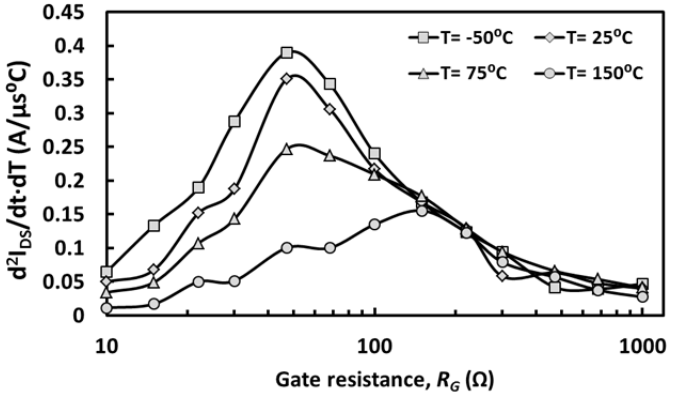

Fig. 11. Measured $d^2I_{DS}/dtdT$ as a function of R_G at different temperatures.

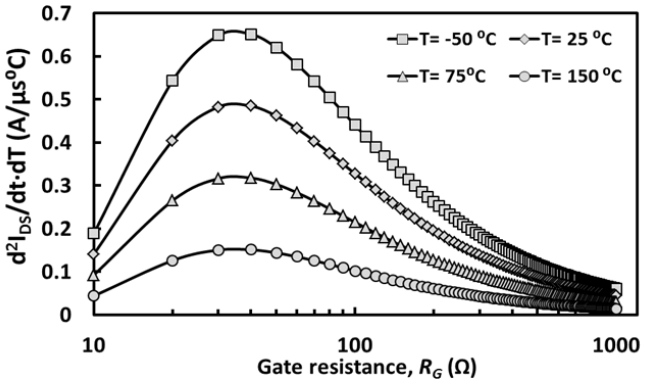

Fig. 12. Calculated $d^2I_{DS}/dtdT$ as a function of R_G at different temperatures.

IV. Diode Switching Analysis

The response of the diode output voltage characteristics to the MOSFET switching is determined primarily by the transfer function of the diode, the gate resistance of the gate driver and the junction temperature of the device. The transfer function of the diode can be determined by the equivalent circuit of the diode which is represented by a series resistance (R_S), diode depletion capacitance (C_{AK}), diode depletion resistance (R_{AK}) and the stray packaging inductance (L_{stray}) as shown in Figure 13. The parasitic capacitance arises from the depletion capacitance of the diode, the series resistance arises from the resistance of the drift region and the stray inductance arises from the packaging.

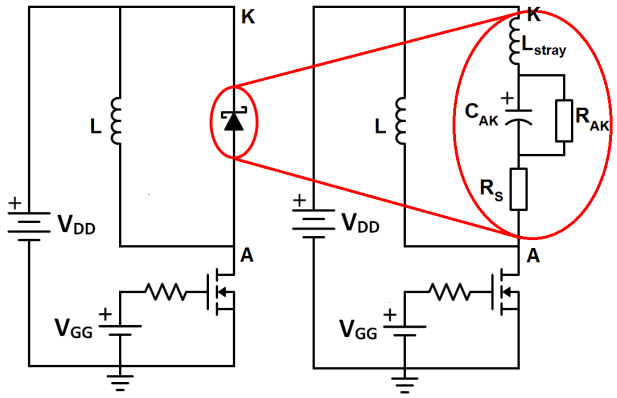

Fig. 13. Circuit schematic of experimental test rig showing the equivalent circuit of the diode.

The diode voltage (V_{AK}) can then be calculated as the product of the diode transfer function and an input function that represents the switching of the MOSFET. This transfer function can be represented by the equation shown below:

$$V_{AK} = \frac{V_{DD}}{1 + sR_GC_{GD}} \times \frac{s\left(\frac{R_S}{L_{Stray}}\right) + \frac{R_{AK} + R_S}{L_{stray}R_{AK}C_{AK}}}{s^2 + s\left(\frac{R_{AK}R_SC_{AK} + L_{stray}}{L_{stray}R_{AK}C_{AK}}\right) + \frac{R_{AK} + R_S}{L_{stray}R_{AK}C_{AK}}} \quad (9)$$

where C_{GD} is the Miller capacitance of the MOSFET. As the MOSFET switches ON, the majority of the supply voltage (V_{DD} in Figure 13) which initially falls across the MOSFET now falls across the diode, thereby reverse biasing the diode. Hence, the action of the MOSFET is identical to a step voltage rise across the diode with the rate of change of voltage with time dependent on the MOSFET switching time constant ($R_G C_{GD}$). The transfer function of the diode is basically that of a second order circuit which can respond as over-damped, under-damped or critically damped depending on the attenuation present. The attenuation and damping of the diode response can be derived as the equations below:

$$\alpha = \frac{R_{AK} R_S C_{AK} + L_{stray}}{2 L_{stray} R_{AK} C_{AK}}$$

$$\zeta = \frac{R_S R_{AK} C_{AK} + L_{Stray}}{2\sqrt{R_S R_{AK} L_{Stray} C_{AK} + R_{AK}^2 L_{Stray} C_{AK}}}$$

The dI_{DS}/dt of the MOSFET at turn-ON will determine the nature of the diode response since the same current flows through the transistor and the diode. Hence, the diode response will depend on the gate resistance and the temperature. Figure 14 and 15 show the MOSFET turn-ON current transient at different temperatures for R_G = 150 Ω in Figure 14 and R_G = 15 Ω in Figure 15.

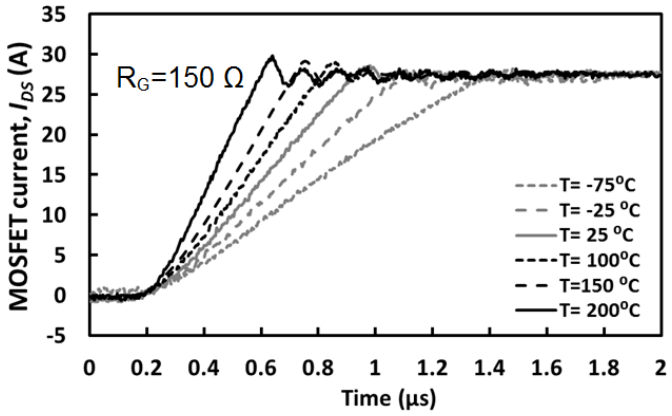

Fig. 14. MOSFET drain current as a function of time during turn-ON at different temperatures with R_G = 150 Ω.

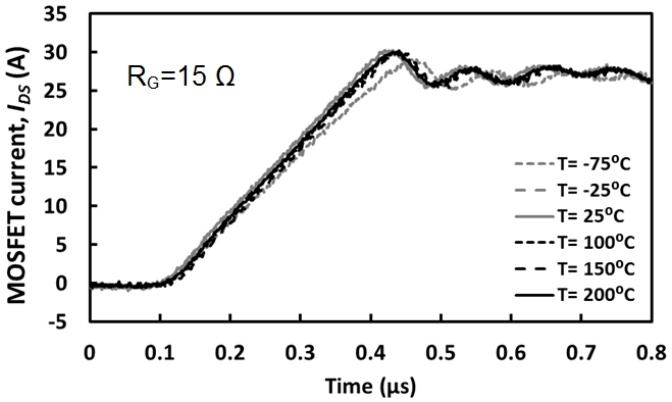

Fig. 15. MOSFET drain current as a function of time during turn-ON at different temperatures with R_G = 15 Ω.

From Figure 14 and Figure 15, it can be seen that the dI_{DS}/dt is more temperature invariant at R_G = 15 Ω than at R_G = 150 Ω; i.e. $d^2I_{DS}/dtdT$ is larger at R_G = 150 Ω in agreement with Figure 11 and Equation (7). It can also be seen from Figure 15 that the turn-ON dI_{DS}/dt increases with temperature according to the equations developed previously. Additionally Figure 16 and 17 show the diode voltage response at the R_G = 150 Ω and R_G = 15 Ω, respectively. It should be noted that the ringing oscillation frequency of the diode at turn-OFF depends strongly on the parasitic inductances which will be unique for a certain power modules and experimental rig. However, the equivalent circuit shown in Figure 13 will be universal for power converters. The most obvious difference between Figure 16 and 17 is the higher V_{AK} variation with temperature exhibited by the R_G = 150 Ω measurements i.e. the R_G = 15 Ω measurements shows less dependence of V_{AK} on temperature. Previous publications have shown a temperature invariance of the SiC Schottky diode turn-OFF characteristics [14]; however, this was demonstrated at low gate resistance (R_G = 2.5 Ω) as is the case in Figure 17. At slower switching rates (larger gate resistances); the dependence of dI_{DS}/dt on temperature affects the diode temperature characteristics as shown in Figure 16 In other words, the rate at which the transistor switches will determine the response of the diode to the discharge of the free-wheeling current. If the diode is discharged very rapidly (high dI_{DS}/dt from low R_G), then the diode will ring with less damping (circuit is excited by a larger $|dV/dt|$, resulting in larger overshoots.) and higher overshoots than if the current is discharged more slowly. The temperature dependence of the diode response also increases as the switching rate is reduced. It can also be noticed in Figure 16 that there is a time shift in the diode response with low temperature characteristics exhibiting a time delay compared to high temperature characteristics. This is due to the negative temperature coefficient of the MOSFETs threshold voltage which means that switching time is delayed at low temperatures (because of the higher MOSFET V_{TH}). Also, it can be seen from these figures that the damping of the oscillations for the 15 Ω measurements is less, peak voltage overshoot is higher and the temperature dependence is smaller compared to the oscillations at 150 Ω gate resistance.

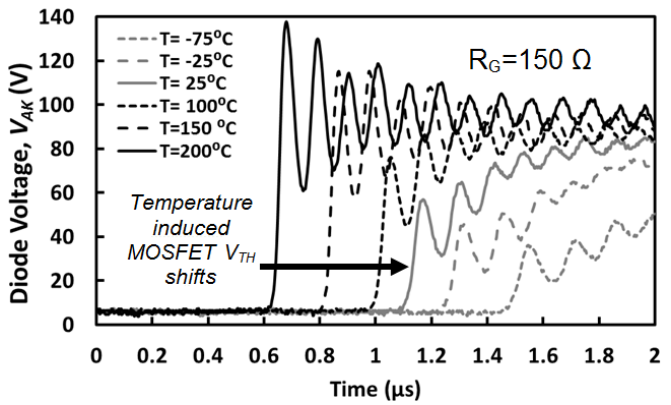

Fig. 16. Measured diode output voltage as a function of time during MOSFET turn-ON at different temperatures with R_G = 150 Ω.

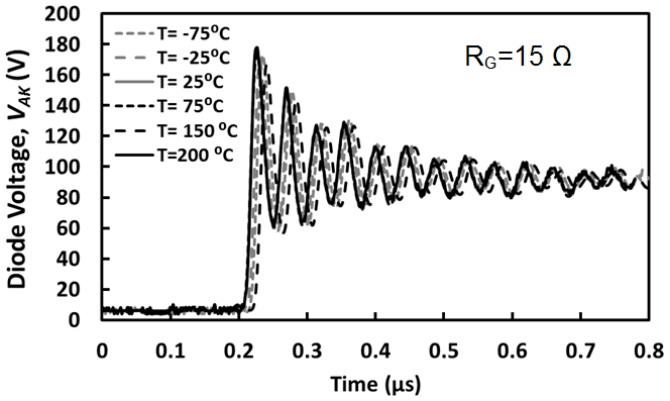

Fig. 17. Measured diode output voltage as a function of time during MOSFET turn-ON at different temperatures with R_G = 15 Ω.

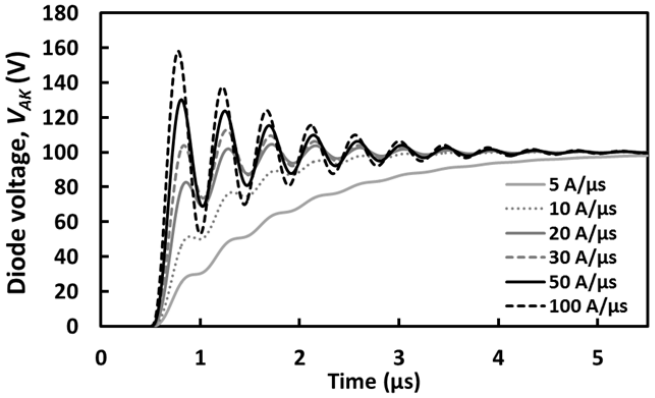

Fig. 18. Calculated diode output voltage as a function of time during MOSFET turn-ON at different dI_{DS}/dt.

This is a direct result of the measurements shown in Figure 14 and 15 because the diode responds to the dI_{DS}/dt of the MOSFET. Also, the dI_{DS}/dt dependence on temperature causes a time shift in the diode response with the high temperature V_{AK} occurring faster. Figures 14 to 17 can be explained by the fact that $d^2I_{DS}/dtdT$ is higher at intermediate R_G values and reduces as R_G is reduced. Combining (9) and (4) yields:

$$V_{AK} = A \times \frac{s\left(\frac{R_S}{L_{Stray}}\right) + \frac{R_{AK}+R_S}{L_{stray}R_{AK}C_{AK}}}{s^2 + s\left(\frac{R_{AK}R_SC_{AK}+L_{stray}}{L_{stray}R_{AK}C_{AK}}\right) + \frac{R_{AK}+R_S}{L_{stray}R_{AK}C_{AK}}} \quad (10)$$

where

$$A = \frac{\frac{\mathrm{d}I_{DS}}{\mathrm{d}t}V_{DD}}{\frac{\mathrm{d}I_{DS}}{\mathrm{d}t} + s\left(\frac{BV_{GG}\left(V_{GS}-V_{TH}\right)}{C_{iss}}C_{GD}\right)}$$

In deriving (10), it is assumed that the MOSFET switching time constant R_GC_{GD} is substantially larger than t, hence, $exp(-t/R_GC_{iss})$ is close to 1.

Equation (10) is a very useful equation because it relates the turn-ON dI_{DS}/dt of the MOSFET to the diode output voltage. Figures 18 shows the simulated plot of (10) using dI_{DS}/dt values similar to what was measured (between 10 and 100 A/μs). The diode depletion capacitance is taken from an average depletion capacitance value determined from CV measurements while R_{AK} is also determined from CV measurements. L_{stray} is varied between 1 and 5 nH while R_S is assumed to be a few milliohms. The effect of R_S and R_{AK} is to dampen the oscillations, while C_{AK} and L_{stray} affect the oscillation frequency. Figures 18 is a reasonably accurate simulation of the diode's switching behavior, however, because all of these parasitic components vary during switching and are difficult to measure, an exact replica of the experimental measurements is difficult to achieve. Figures 18 also shows that increasing turn-ON dI_{DS}/dt (which can result from either a lower gate resistance or higher ambient temperatures) causes higher V_{AK} peak overshoots and more diode ringing.

Figures 19 and 20 show 3D plots of the measured switching energy at turn-OFF and ON for the SiC Schottky diode at different dI_{DS}/dt and temperatures. The dI_{DS}/dt shown in this figure, is calculated at 25 °C. It can be seen from the figures that the diode turn-OFF energy is significantly larger than the turn-ON energy. It can also be seen from Figures 19 and 20 that for a given dI_{DS}/dt (or gate resistance), the switching energy reduces with increasing temperature during diode turn-OFF. This is due to the fact that MOSFET switching rates increases with temperature in the MOSFET as shown in Figures 7 and the response of the diode is modulated by the switching of the MOSFET as shown in (10). Figures 19 and 20 show that the dependence of the switching energy on the gate resistance exhibits a U shaped characteristic with the lowest switching energies at intermediate R_G values. At the lowest R_G, the switching energy is dominated by additional losses from diode ringing, whereas at the highest R_G, the switching energy is due to the prolonged transient. Hence, although using small gate resistances increases the dI_{DS}/dt, the ringing that results can increase the switching energy.

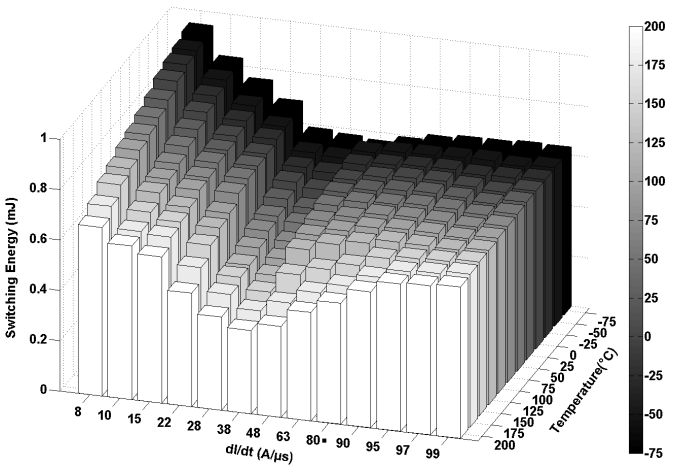

Fig. 19. 3D plots of the SiC Schottky diode switching energy as a function of room temperature dI_{DS}/dt and temperature at turn-OFF.

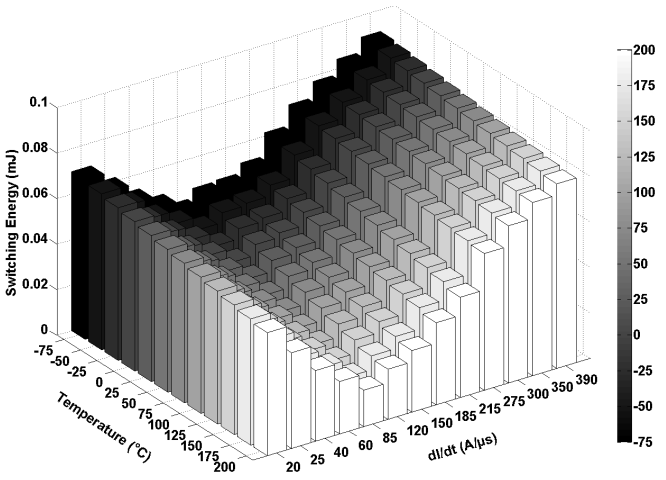

Fig. 20. 3D plots of the SiC Schottky diode switching energy as a function of room temperature dI_{DS}/dt and temperature at turn-ON.

V. Conclusion

The dI_{DS}/dt and temperature dependence of the switching performance of SiC Schottky diodes has been presented over a wide temperature and dI_{DS}/dt range. It is shown that the switching energy as a function of the gate resistance exhibits a U shaped characteristic with switching energy at low R_G dominated by diode ringing losses and at high R_G dominated by transient overlap between V_{AK} and I_{AK}. Diode voltage turn-OFF ringing has been shown to increase with temperature for a fixed gate resistance due to the fact the dI_{DS}/dt increases with temperature during MOSFET turn-ON. It was also shown that the rate of increase of the turn-ON dI_{DS}/dt with temperature increases with the gate resistance. This resulted in greater diode V_{AK} dependence on temperature for higher gate resistances. Device physics based models that explain the experimental observations were developed and were shown to account for the measurements. These results are important because they can account for electromagnetic oscillations as a function of temperature and dI_{DS}/dt, which in turn is important for determining EMI, operating temperature and device reliability.

References

[1] J. Hudgins, "Power electronic devices in the future," *IEEE Jour. Emerg. and Selec. Topics in Power Electron.*, vol. 1, no. 1, pp. 11–17, March 2013.

[2] M. Das, C. Capell, D. Grider, R. Raju, M. Schutten, J. Nasadoski, S. Leslie, J. Ostop, and A. Hefner, "10 kv, 120 a sic half h-bridge power mosfet modules suitable for high frequency, medium voltage applications," *IEEE Energ. Conver. Cong. and Expo. (ECCE)*, pp. 2689–2692, Sept 2011.

[3] S.-H. Ryu, S. Krishnaswami, M. O'Loughlin, J. Richmond, A. Agarwal, J. Palmour, and A. Hefner, "10-kv, 123-m omega; middot;cm2 4h-sic power dmosfets," *IEEE Electr. Devi. Lette.*, vol. 25, no. 8, pp. 556–558, Aug 2004.

[4] H. Mantooth, M. Glover, and P. Shepherd, "Wide bandgap technologies and their implications on miniaturizing power electronic systems," *IEEE Jour. Emerg. and Selec. Topics in Power Electron.*, vol. PP, no. 99, pp. 1–1, 2014.

[5] D. Jiang, R. Burgos, F. Wang, and D. Boroyevich, "Temperature-dependent characteristics of sic devices: Performance evaluation and loss calculation," *IEEE Trans. Power Electr.*, vol. 27, no. 2, pp. 1013–1024, Feb 2012.

[6] Z. Wang, X. Shi, Y. Xue, L. Tolbert, F. Wang, and B. Blalock, "Design and performance evaluation of overcurrent protection schemes for silicon carbide (sic) power mosfets," *IEEE Trans. Ind. Electron.*, pp. 1–1, 2014.

[7] H. Zhang and L. Tolbert, "Efficiency impact of silicon carbide power electronics for modern wind turbine full scale frequency converter," *IEEE Trans. Ind. Electron.*, vol. 58, no. 1, pp. 21–28, Jan 2011.

[8] M. Hernando, A. Fernandez, J. Garcia, D. Lamar, and M. Rascon, "Comparing si and sic diode performance in commercial ac-to-dc rectifiers with power-factor correction," *IEEE Trans. Ind. Electron.*, vol. 53, no. 2, pp. 705–707, April 2006.

[9] B. Zhao, Q. Song, and W. Liu, "Experimental comparison of isolated bidirectional dcdc converters based on all-si and all-sic power devices for next-generation power conversion application,," *IEEE Trans. Ind. Electron.*, vol. 61, no. 3, pp. 1389–1393, March 2014.

[10] J. Biela, M. Schweizer, S. Waffler, and J. Kolar, "Sic versus sievaluation of potentials for performance improvement of inverter and dcdc converter systems by sic power semiconductors,," *IEEE Trans. Ind. Electron.*, vol. 58, no. 7, pp. 2872–2882, July 2011.

[11] H. Sarnago, O. Lucia, A. Mediano, and J. Burdio, "A class-e direct acac converter with multicycle modulation for induction heating systems,," *IEEE Trans. Ind. Electron.*, vol. 61, no. 5, pp. 2521–2530, May 2014.

[12] B. Zhao, Q. Song, W. Liu, and S. Yandong, "A synthetic discrete design methodology of high-frequency isolated bidirectional dc-dc converter for grid-connected battery energy storage system using advanced components," *IEEE Trans. Ind. Electron.*, vol. PP, no. 99, pp. 1–1, 2014.

[13] S. Jahdi, O. Alatise, C. Fisher, L. Ran, and P. Mawby, "An evaluation of silicon carbide unipolar technologies for electric vehicle drive-trains," *IEEE Jour. Emerg. and Selec. Topics in Power Electron.*, vol. PP, no. 99, pp. 1–1, 2014.

[14] O. Alatise, N.-A. Parker-Allotey, D. Hamilton, and P. Mawby, "The impact of parasitic inductance on the performance of silicon carbide schottky barrier diodes," *IEEE Trans. Power Electron.*, vol. 27, no. 8, pp. 3826–3833, Aug 2012.

[15] M. Adamowicz, S. Giziewski, J. Pietryka, and Z. Krzeminski, "Performance comparison of sic schottky diodes and silicon ultra fast recovery diodes," *IEEE Compatibi. and Power Electron. (CPE),*, pp. 144–149, June 2011.

[16] M. Adamowicz, S. Giziewski, J. Pietryka, M. Rutkowski, and Z. Krzeminski, "Evaluation of sic jfets and sic schottky diodes for wind generation systems," *IEEE Inter. Symp. Ind. Electron. (ISIE)*, pp. 269–276, June 2011.

[17] T. Salem and R. Wood, "1000-h evaluation of a 1200-v, 880-a all-sic dual module," *IEEE Trans. Power Electron.*, vol. 29, no. 5, pp. 2192–2198, May 2014.

[18] O. Alatise, N.-A. Parker-Allotey, and P. Mawby, "Modeling the electrothermal stability of power mosfets during switching transients," *IEEE Electr. Dev. Letters*, vol. 33, no. 7, pp. 1039–1041, July 2012.

[19] I. H. Kang, S. Kim, W. Bahng, S. Joo, and N. K. Kim, "Accurate extraction method of reverse recovery time and stored charge for ultrafast diodes," *IEEE Trans. Power Electron.*, vol. 27, no. 2, pp. 619–622, Feb 2012.

[20] W. Wondrak, R. Held, E. Niemann, and U. Schmid, "Sic devices for advanced power and high-temperature applications," *IEEE Trans. Ind. Electron.*, vol. 48, no. 2, pp. 307–308, Apr 2001.

[21] M. Werner and W. Fahrner, "Review on materials, microsensors, systems and devices for high-temperature and harsh-environment applications," *IEEE Trans. Ind. Electron.*, vol. 48, no. 2, pp. 249–257, Apr 2001.

[22] P. Godignon, X. Jorda, M. Vellvehi, X. Perpina, V. Banu, D. Lopez, J. Barbero, P. Brosselard, and S. Massetti, "Sic schottky diodes for harsh environment space applications," *IEEE Trans. Ind. Electron.*, vol. 58, no. 7, pp. 2582–2590, July 2011.

[23] R. Wang, D. Boroyevich, P. Ning, Z. Wang, F. Wang, P. Mattavelli, K. Ngo, and K. Rajashekara, "A high-temperature sic three-phase ac - dc converter design for 100 deg c ambient temperature," *IEEE Trans. Power Electron.*, vol. 28, no. 1, pp. 555–572, Jan 2013.

[24] T. Funaki, J. Balda, J. Junghans, A. Kashyap, H. Mantooth, F. Barlow, T. Kimoto, and T. Hikihara, "Power conversion with sic devices at extremely high ambient temperatures," *IEEE Trans. Power Electron.*, vol. 22, no. 4, pp. 1321–1329, July 2007.

[25] J. Baliga, *Fundamentals of Power Semiconductor Devices*. Springer, 2010.

[26] Z. Chen, Y. Yao, M. Danilovic, and D. Boroyevich, "Performance evaluation of sic power mosfets for high-temperature applications," *IEEE Power Electron. and Motion Contr. Conf.*, pp. 1–9, Sept 2012.

[27] Z. Chen, Y. Yao, D. Boroyevich, K. Ngo, P. Mattavelli, and K. Rajashekara, "A 1200 v, 60 a sic mosfet multi-chip phase-leg module

for high-temperature, high-frequency applications," *IEEE Appli. Power Electron. Conf. and Expo. (APEC)*, pp. 608–615, March 2013.

[28] K. Takao, S. Harada, T. Shinohe, and H. Ohashi, "Performance evaluation of all sic power converters for realizing high power density of 50 w/cm3," *IEEE Power Electron. Conf. (IPEC)*, pp. 2128–2134, June 2010.

Saeed Jahdi (S'10) received the BSc degree in Electrical Power Engineering from University of Science and Technology, Tehran, Iran, in 2005 and the degree of MSc with distinction in Power Systems and Energy Management from City University London, U.K., in 2012. Since then, he is pursuing the Ph.D. degree in electrical engineering as a candidate in Power Electronics laboratory of School of Engineering of University of Warwick, U.K. while he has been awarded an energy theme scholarship for the duration of his research. His current research interests include wide band-gap semiconductor devices in high voltage power converters, circuits and applications. Mr. Jahdi is a member of IEEE Power Electronics and Industrial Electronics societies.

Olayiwola Alatise received the B.Eng. degree (with first-class honors) in electrical engineering and the Ph.D. degree in microelectronics and semiconductors from Newcastle University, Newcastle upon Tyne, U.K., in 2008. His research focused on mixed-signal performance enhancements in strained Si/SiGe metaloxidesemiconductor field-effect transistors (MOSFETs). In 2004 and 2005, he briefly joined Atmel North Tyneside, where he worked on the process integration of the 130-nm CMOS technology node. In June 2008, he joined the Innovation R&D Department, NXP Semiconductors, as a Development Engineer, where he designed, processed, and qualified discrete power trench MOSFETs for automotive applications and switched-mode power supplies. In November 2010, he became a Science City Research Fellow with the University of Warwick and since August 2012, he is serving as assistant professor of electrical engineering in University of Warwick, U.K. His research interest include investigating advanced power semiconductor materials and devices for improved energy conversion efficiency.

Petros Alexakis (S'12) received the BSc degree in Physics from Aristotle University of Thessaloniki in 2010 with a major in Electronics and Telecommunications and the MSc degree with merit in Renewable Energy and Power Electronics from the School of Engineering of University of Warwick in 2012. He also worked as a private tutor teaching Physics and Math as well as an Electrical Engineer in the Greek Navy. He is currently pursuing his Ph.D. in electrical engineering and more specifically in wide bandgap semiconductor devices in PEATER group in the School of Engineering of University of Warwick. He has been awarded an EPSRC scholarship for the duration of his research. His current research interests include modelling of wide band-gap semiconductor devices, reliability and ruggedness. Mr. Alexakis is a student member of IEEE.

Li Ran (M'98-SM'07) received a PhD degree in Power Systems Engineering from Chongqing University, Chongqing, China, in 1989. He was a Research Associate with the Universities of Aberdeen, Nottingham and Heriot-Watt, at Aberdeen, Nottingham and Edinburgh in the UK respectively. He became a Lecturer in Power Electronics with Northumbria University, Newcastle upon Tyne, the UK in 1999 and was seconded to Alstom Power Conversion, Kidsgrove, the UK in 2001. Between 2003 and 2012, he was with Durham University, Durham, the UK. He joined the University of Warwick, Coventry, UK as a Professor in Power Electronics - Systems in 2012. His research interests include the application of Power Electronics for electric power generation, delivery and utilisation.

Philip Mawby (S'85-M'86-SM'01) received the B.Sc. and Ph.D. degrees in electrical engineering from the University of Leeds, U.K., in 1983 and 1987, respectively. His Ph.D. thesis was focused on GaAs/AlGaAs heterojunction bipolar transistors for high-power radio frequency applications at the GEC Hirst Research Centre, Wembley, U.K.

In 2005, he joined the University of Warwick, U.K. as the Chair of power electronics. He was with the University of Wales for 19 years and held the Royal Academy of Engineering Chair for power electronics, where he established the Power Electronics Design Center. He has coauthored more than 100 journal and conference papers. His current research interests include materials for new power devices, modeling of power devices and circuits, and power integrated circuits. He is a Chartered Engineer, a Fellow of the Institution of Engineering and Technology, and a Fellow of the Institute Physics. He is a Distinguished Lecturer for the IEEE Electron Devices Society.